

The nuclear bulge of the Galaxy

II. The K band luminosity function of the central 30 pc

P.G. Mezger¹, R. Zylka^{2,1}, S. Philipp¹, and R. Launhardt¹

¹ Max-Planck-Institut für Radioastronomie, Auf dem Hügel 69, D-53121 Bonn, Germany

² Institut für Theoretische Astrophysik, Tiergartenstrasse 15, D-69121 Heidelberg, Germany

Received 19 January 1999 / Accepted 4 June 1999

Abstract. Philipp et al. (1999, Paper I) investigated the K band emission from a mosaic of size $\Delta\alpha \times \Delta\delta \sim 650'' \times 710''$ centered approximately on Sgr A* ($R_{\text{equiv}} \sim 15.8$ pc for $R_0 = 8.5$ kpc). For the $\sim 6 \times 10^4$ stars above the detection limit ($S'_K \sim 100 \mu\text{Jy}^1$) an *observed* K -band luminosity function (KLF) has been obtained. Below the completeness limit ($S'_K \sim 2000 \mu\text{Jy}$), an ever increasing fraction of stars merges into the background continuum. In this paper we combine the *observed* with *model* KLFs and thus obtain a *complete* KLF for the flux density range $3 \times 10^{-3} \gtrsim S'_K/\mu\text{Jy} \gtrsim 2 \times 10^6$. The overall KLF consists of four sectors obeying power laws of the form $dN(S'_K)/d\log S'_K \propto S'^{\gamma_1+1}$, where $\gamma_1 + 1$ decreases from -0.6 to -1.75 . Sector I corresponds to a Salpeter Initial Mass Function (IMF) and represents Main Sequence (MS) stars with $M_* \lesssim 1 M_\odot$, which account for $\sim 90\%$ of the dynamical mass but only $\sim 6\%$ of the K band flux density. Sector II represents MS stars with $M_* \gtrsim 1 M_\odot$ and red giants. These stars account for only $\sim 6\%$ of the dynamical mass and a similar percentage of the integrated K -band surface brightness but represent $\sim 80\%$ of the bolometric stellar luminosity in the mosaic. The Mass Function (MF) of MS stars is $dN/dM_* \propto M_*^{-2.35}$ (i.e., the Salpeter IMF) for $M_* \lesssim 1 M_\odot$ and $dN/dM_* \propto M_*^{-4.5}$ for more massive stars, which is similar to the Present Day MF in the solar vicinity. Part of sector II of the KLF, as well as sectors III and IV, represent giants and supergiants which, though they account for only a small fraction of the mass, dominate the integrated K -band surface brightness.

The slope of sector II of the KLF, $\gamma_1 + 1 \sim -0.8$ has been inferred from the KLF in the NGC 6522 Baade's Window (BW). To make this sector join smoothly to the neighboring KLF sections we have to set the surface density of low-mass ($\sim 1 M_\odot$) MS stars at ~ 56 times that in BW.

Paper I shows, in agreement with earlier observations, that massive stars are preferentially formed in the central parsec. A preliminary discussion of star formation rates suggests that bimodal star formation (introduced by Güsten & Mezger [1983] for the spiral arm region of the Galactic Disk) may also apply

to the central 30 pc. Preferential formation of stars with masses $M_* \gtrsim M_c \sim 1\text{--}5 M_\odot$ would make conversion of matter into radiation by star formation much more efficient and could be the process which powers star burst galaxies. There is an overabundance of evolved stars which can be explained by a strongly increased star formation rate $\sim 10^8\text{--}10^9$ yrs ago.

Key words: stars: luminosity function, mass function – ISM: dust, extinction – Galaxy: center – Galaxy: evolution – Galaxy: stellar content – infrared: stars

1. Introduction

In a recent review (Mezger et al., 1996; hereafter MDZ96) we have compared the central region of our galaxy with active nuclei in external galaxies and have found that it belongs to the class of mildly active Seyfert nuclei, which fuel their luminosity by starbursts and account for $\sim 10\%$ of all spiral galaxies. The conclusion is nearly inevitable that there is a black hole of mass $\sim 2.6 \times 10^6 M_\odot$ at the center of our galaxy, coinciding with the compact radio source Sgr A* (Genzel et al., 1997, and references therein). However, all observations agree that accretion onto this black hole does not at present contribute more than a few hundred L_\odot to the dust luminosity of $\sim 4 \times 10^6 L_\odot$ of the central parsec, which is mainly powered by the absorption of radiation from massive young stars.

Are there indications of greater activity in the past? Apart from the enigmatic source Sgr A East, there are few observations supporting recent violent energy releases which could be connected to the black hole. It rather appears that the ISM is swept by a bar from the Galactic Disk (GD) towards the Center, where it assembles in a disk-like structure of stars and ISM referred to as the Nuclear Bulge (NB). The bar, on the other hand, is identified with the Galactic Bulge (GB) which extends in the galactic plane as far as $R \sim 3.5$ kpc. Episodic star formation, i.e. the more or less periodic transformation of the inward flowing ISM into stars, appears to account for most of the more recent activity in the Galactic Center (see also Serabyn & Morris, 1996). Within the inner Lindblad resonance of the GD, i.e. $R \lesssim 3.5$ kpc, star formation occurs nearly exclusively in the NB which – as seen both in the starlight dominated near-in-

Send offprint requests to: P.G. Mezger, Bonn

Correspondence to: sphilipp@mpifr-bonn.mpg.de

¹ In the following we refer to S'_v as observed and S_v as dereddened flux density.

Table 1. Abbreviations used in this paper

abbreviations	meaning
BW	Baade's Window, an area of low extinction centered approximately at $l \sim 1^\circ$, $b \sim -3.9^\circ$
GB	Galactic Bulge
GC	Galactic Center
GD	Galactic Disk
IMF	Initial Mass Function
KLF	K band Luminosity Function
LF	Luminosity Function
Lyc	Lyman Continuum
MF	Mass Function
Mosaic	Area of size $\Delta\alpha \times \Delta\delta \sim 650'' \times 710''$ centered approximately on Sgr A *
MS	Main Sequence
NB	Nuclear Bulge
PDMF	Present Day Mass Function
SFR	Star Formation Rate

frared ($\lambda \lesssim 5\text{--}7 \mu\text{m}$) and in the dust emission dominated mid-to far-infrared – extends $\sim 200\text{--}300$ pc in the galactic plane and $\sim 30\text{--}50$ pc perpendicular to it and may be adequately described as a massive ($\sim 4 \times 10^9 M_\odot$) disk or torus consisting of stars and interstellar matter. The physical conditions in the NB – specifically the matter and radiation densities – are extreme: In a volume $V_{\text{NB}} \sim 10^{-4} V_{\text{GD}}$ the NB contains $\sim 5\%$ of the total mass of stars and ISM in the GD. Similar percentages hold for the stellar and dust luminosities. To further investigate its evolution we have begun a program to investigate the physical state of the NB. In Paper I (Philipp et al., 1999), we derived the K -band luminosity function (KLF) of the central ~ 30 pc, which we here analyze and interpret it in terms of star formation history. The star formation history of the NB will be dealt with in a later paper.

To keep this paper concise we have used a number of abbreviations whose meanings are explained in Table 1.

2. Observations

A visual extinction of typically ~ 31 mag caused by dust in the GD and NB (the GB to a first approximation is free of dust) prevents observations of stars in the NB at wavelengths $\lambda < 1.6 \mu\text{m}$. We have constructed mosaic images in the H - and K -bands ($\lambda 1.65$ and $2.2 \mu\text{m}$) of an area $\Delta\alpha \times \Delta\delta \sim 650'' \times 710''$ (equivalent radius $R_{\text{eq}} \sim 383''$ or 15.8 pc for $R_0 = 8.5$ kpc),² centered approximately on Sgr A *. In Paper I (Philipp et al., 1999) we reported on results obtained from the K -band mosaic. With a detection limit $S'_K \sim 100 \mu\text{Jy}$ ³ and a completeness limit of $S'_K \gtrsim 2000 \mu\text{Jy}$, we separated $\sim 6 \times 10^4$ sources from an extended unresolved background and derived a logarithmic K -band luminosity function (KLF) $dN(S'_K)/d\log S'_K \propto S'^{\gamma_1+1}$

² Here we use “mosaic” and “central 30 pc” as synonymous expressions.

³ In the following we refer to S'_K as observed and S_K as dereddened K -band flux densities.

which increases with $\gamma_1 + 1 \sim -1.75$ for $2 \times 10^6 \gtrsim S'_K/\mu\text{Jy} \gtrsim 4.5 \times 10^4$, flattens to $\gamma_1 + 1 \sim -1.0$ for $4.5 \times 10^4 \gtrsim S'_K/\mu\text{Jy} \gtrsim 3.6 \times 10^3$ and attains a maximum at $S'_K \sim 4 \times 10^3 \mu\text{Jy}$.

Fig. 9 of Paper I shows computed and reddened K -band flux densities of Main Sequence (MS), giant and supergiant stars. It is clear from this diagram that only giants, supergiants and MS stars earlier than B5 are observable above the detection limit. MS stars later than B5 and a decreasing number of stars with S'_K between the detection and completeness limits are not detected as individual sources but merge into the background continuum. In Paper I we find that, of a flux density of $S'_{K,\text{integr}} \sim 752$ Jy integrated over the mosaic, about half is contributed by stars above the detection limit and the other half is contributed by the background continuum. We also estimate that a flux density $S'_{\text{GB+GD}} \sim 131$ Jy is contributed to $S'_{K,\text{integr}}$ by stars in Galactic Bulge and Disk.

3. Interrelations between mass and luminosity functions

The logarithmic K -band luminosity function (KLF) $dN(S'_K)/d\log S'_K$ counts the number of sources within a given flux density range in logarithmic bins. This allows a convenient graphical presentation of data taken over as many as 8 decades. For numerical evaluations a linear KLF $dN(S')/dS'_K$ (i.e. with sources counted in linear bins) is, however, more convenient. There exists the relation

$$\frac{dN}{dS'_K} = 0.43 S'^{-1} \frac{dN(S'_K)}{d\log S'_K}. \quad (1)$$

For ease in making comparisons one usually normalizes observed KLFs to an area of $1''$. Here we discuss luminosity and mass functions relating to the mosaic and thus have to multiply the above equation by $\Omega_{\text{mosaic}} \sim 4.1 \times 10^{5\prime\prime}$, the solid angle that it subtends. We thus have

$$\begin{aligned} \frac{dN(\text{mosaic})}{dS'_K} &= 0.43 \Omega_{\text{mosaic}} S'^{-1} \frac{dN(S'_K)}{d\log S'_K} \\ &= C_1 S'^{\gamma_1}. \end{aligned} \quad (2)$$

In Paper I we showed that a mass function (MF) – in this case the Salpeter Initial Mass Function (IMF)

$$\frac{dN}{dM_*} = AM_*^\alpha, \quad (3)$$

where $\alpha = -2.35$, can be transformed into a model KLF given by the above relation (2) with $\gamma_1 = -1.6$, using the observed relation between stellar mass and reddened K -band flux density

$$\left(\frac{S'_K}{\mu\text{Jy}}\right) \sim 1.6 \left(\frac{M_*}{M_\odot}\right)^{2.3} = B_1 M_*^{\beta_1}. \quad (4)$$

With the stellar parameters given in Appendix A this relation holds approximately for all Main Sequence (MS) stars.

In a similar way the luminosity function (LF), i.e. the distribution function of the total stellar luminosity

$$\frac{dN}{dL_*} = C_2 L_*^{\gamma_2} \quad (5)$$

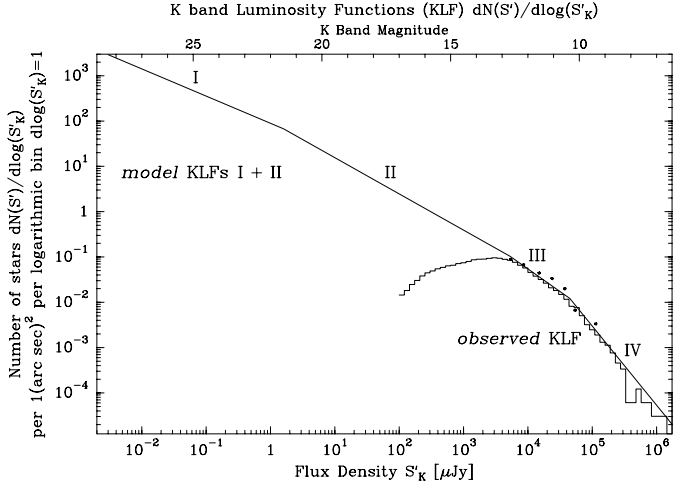


Fig. 1. The complete mosaic KLF is shown together with the observed KLF and datapoints of the luminous part of the adjusted BW KLF (Tiede et al., 1995, and references therein). See also Sect. 4.3.

can be constructed with

$$\frac{L_*}{L_\odot} = B_2 M_*^{\beta_2} = \begin{cases} M_*^{2.8} & \text{for } M_* \lesssim 1 M_\odot \\ M_*^4 & \text{for } M_* \gtrsim 1 M_\odot \end{cases} \quad (6)$$

which is valid for MS stars (see e.g. Lang, 1992). Relations showing how to compute the numerical values A or C and the exponents α or γ with $B_1 = 1.6$, $B_2 = 1$ and $\beta_2 = 2.8$, and 4, respectively, can be found in Appendix B. They can be used to convert K -band luminosity functions into mass and bolometric luminosity functions.

4. A complete mosaic KLF

A complete mosaic KLF is shown in Fig. 1 and given in Table 2 in analytical form. It consists of four sectors described by power-law approximations of the form $dN(S'_K)/d\log S'_K \propto S'^{\gamma_1+1}$. Here $\gamma_1 + 1$ increases from -1.75 to -0.6 while S'_K decreases from 2×10^6 to $3 \times 10^{-3} \mu\text{Jy}$.

The four sectors are labeled I through IV and are listed in Column 1 of Table 2. Column 2 gives their ranges of validity. Power law approximations $dN(S'_K)/d\log S'_K$, normalized to an area of $1''$, are given in Column 3 and shown in Fig. 1. The corresponding linear KLFs $dN(S'_K)/dS'_K$, but now referred to the mosaic with $\Omega_{\text{mosaic}} \sim 4.1 \times 10^{5\hat{n}}$, are given in Column 4. Stellar luminosity (LF) and mass functions (MF) related to the mosaic are given in Columns 8 and 10. Column 7 delineates the range of MS stellar masses to which the MFs apply. Cumulative numbers of stars and their reddened K band flux densities are given in Columns 5 and 6, while cumulative stellar luminosities and masses are given in Columns 9 and 11.

4.1. Conditions a complete mosaic KLF must comply with

As mentioned in Sect. 2, the $\sim 6 \times 10^4$ sources with reddened flux densities above the detection limit $S'_K \sim 100 \mu\text{Jy}$ account for only about half of the flux density integrated over the mosaic.

The weaker sources form a continuum for which one has to find an appropriate model KLF. This model KLF should comply with the following conditions:

1. It should smoothly join with the observed KLF above the completeness limit.
2. It should be physically plausible.
3. The cumulative flux density must agree with

$$\begin{aligned} S'_{\text{cum}} &= \int_{S'_K=3 \times 10^{-3} \mu\text{Jy}}^{2 \times 10^6 \mu\text{Jy}} S'_K \frac{dN}{S'_K} dS'_K \\ &= S'_{K,\text{integr}} \sim 752 \text{ Jy}, \end{aligned} \quad (7)$$

the K -band flux density integrated over the mosaic. The sum at the bottom of Column 6 Table 2 shows that the cumulative flux density of the complete KLF actually agrees within $< 1\%$ with the integrated flux density.

4.2. The model KLF $dN_{\text{I}}(S'_K)/d\log S'_K$ based on the Salpeter IMF

In Paper I we adopted the Salpeter IMF (see Table 2, Column 10, sector I) and converted it into the KLF $\propto S'^{-0.6}$ (Column 3). The IMF describes the mass distribution of a newly formed generation of stars; hence, the use of an IMF is physically plausible only for stars with masses $M_* \lesssim 1 M_\odot$ (or $S'_K \lesssim 1.6 \mu\text{Jy}$) whose MS lifetime $\tau_{\text{MS}} \gtrsim 10^{10}$ yrs is the assumed age of the NB. This determines the range of validity as given in Table 2, Column 2 for the KLF in sector I.

4.3. The model KLF $dN_{\text{II}}(S'_K)/d\log S'_K$ based on observations in Baade's Window

The NGC 6522 Baade's Window (BW) located at $l \sim 1^\circ$, $b \sim -3.9^\circ$ is distinguished by its low extinction ($A_K \sim 0.13$ mag) compared to $A_K \sim 3.5$ mag in the direction of the Galactic Center. The BW KLF has been the subject of a number of investigations by Davidge et al. (1997), DePoy et al. (1993) and Tiede et al. (1995). We use the latter's KLF, which appears to be complete for $K_0 \lesssim 16.25$ mag; it is given as number of stars per $0.5 m_K$ in an area of 2.58 arcmin^2 . After conversion of K magnitudes into reddened (by $A_K \sim 0.13$ mag) flux densities $S'_{K,\text{BW}}$ and normalization to an area of $1''$ we obtain the following observed logarithmic BW KLF:

$$\frac{dN(\text{BW})}{d\log S'_{K,\text{BW}}} = 21.15 S'^{-0.80}_{K,\text{BW}} \quad (8)$$

valid within the limits $m_K \sim 9.75$ and 16.25 mag or $8 \times 10^4 \gtrsim S'_{K,\text{BW}}/\mu\text{Jy} \gtrsim 2 \times 10^2$. For a comparison with the mosaic KLF one has to compensate the BW KLF for the extra reddening towards the GC, using the relation $S'_{K,\text{mosaic}} = e^{-\tau_K} S'_{K,\text{BW}}$. For $A_{K,\text{mosaic}} \sim 3.5$ mag and $A_{K,\text{BW}} \sim 0.13$ mag one obtains $\tau_K \sim 3.1$ and $S'_{K,\text{mosaic}} \sim 4.5 \times 10^{-2} S'_{K,\text{BW}}$, which, when substituted into Eq. (8), yields

$$\text{KLF}(\text{BW, reddened}) \sim 1.77 S'^{-0.80}_{K,\text{mosaic}} \quad (9)$$

Table 2. Mass and luminosity functions of the central 30 pc

Sector	$S'_{K,\min}, S'_{K,\max}$ μJy	$dN(S'_K)/d\log S'_K$ S'_K in μJy	$dN(S'_K)/dS'_K$ S'_K in μJy	N_{cum}	S'_{cum} Jy	
(1)	(2)	(3)	(4)	(5)	(6)	
I	$3 \cdot 10^{-3}$	1.6	$89.6 S'_K{}^{-0.6}$	$1.58 \cdot 10^7 S'_K{}^{-1.6}$	$8.4 \cdot 10^8$	43.8
II	1.6	$5.3 \cdot 10^3$	$98.4 S'_K{}^{-0.8}$	$1.73 \cdot 10^7 S'_K{}^{-1.8}$	$1.5 \cdot 10^7$	385.7
IIa	1.6	$5.3 \cdot 10^3$	$136.1 S'_K{}^{-1.5}$	$2.40 \cdot 10^7 S'_K{}^{-2.5}$	$(7.9 \cdot 10^6)$	(37)
III	$5.3 \cdot 10^3$	$4.5 \cdot 10^4$	$547 S'_K{}^{-1.0}$	$9.64 \cdot 10^7 S'_K{}^{-2.0}$	$1.6 \cdot 10^4$	206.2
IV	$4.5 \cdot 10^4$	$2 \cdot 10^6$	$1.69 \cdot 10^6 S'_K{}^{-1.75}$	$2.98 \cdot 10^{11} S'_K{}^{-2.75}$	$1.2 \cdot 10^3$	121.1
$\Sigma_{\text{I}}^{\text{IV}}$					$8.6 \cdot 10^8$	756.8

Sector	$M_{*,\min}, M_{*,\max}$ M_{\odot}	dN/dL_* L_* in L_{\odot}	$L_{*,\text{cum}}$ L_{\odot}	dN/dM_* M_* in M_{\odot}	$M_{*,\text{cum}}$ M_{\odot}
(1)	(7)	(8)	(9) [a], [b]	(10)	(11) [a]
I	0.06	1	$9.75 \cdot 10^6 L_*^{-1.50}$	$1.5 \cdot 10^7 M_*^{-2.35}$	$1.3 \cdot 10^8$
II	1	34	$6.83 \cdot 10^6 L_*^{-1.45}$	$(2.9 \cdot 10^{10}) M_*^{-2.85}$	$(3.1 \cdot 10^7)$
IIa	1	34	$6.83 \cdot 10^6 L_*^{-1.9}$	$2.8 \cdot 10^8 M_*^{-4.5}$	$8.2 \cdot 10^6$
III			$\gtrsim 4.2 \cdot 10^7$		
IV			$\gtrsim 2.1 \cdot 10^7$		
$\Sigma_{\text{I}}^{\text{IV}}$			$\gtrsim 3.6 \cdot 10^8$		$1.4 \cdot 10^8$

[a] Values in brackets have not been used to compute $\Sigma_{\text{I}}^{\text{IV}}$.

[b] Cumulative luminosities I, II, and IIa have been computed by integration of the LF, Column 8, within the limits $3.8 \times 10^{-4} - 1 L_{\odot}$ for sector I and $1 - 1.3 \times 10^6 L_{\odot}$ for sector II; luminosities related to sectors III and IV have been computed by substituting $T_{\text{eff}} \sim 3000$ K and S'_{cum} from Column 6 in Eq. (11), the contribution of evolved stars to the stellar luminosity of sector II has been neglected.

Since we have fixed the slope of the KLF at $\gamma_1 + 1 = -0.80$ the only free parameter available to adjust the modified BW KLF to the KLF in sector I (see previous section) is the surface density N_* of MS stars at $M_* \sim 1 M_{\odot}$. We obtain the best fit approximation, as given in Table 2, Column 3, sector II, by multiplying the above relation by

$$\frac{N_*(\text{mosaic})}{N_*(\text{BW})} = \frac{98.4}{1.77} = 55.6 \quad (10)$$

The corresponding space-averaged volume density is $n_*(NB) \sim 10^3 n_*(GB)$. The observed KLF, shifted to the mosaic, is valid in the range $9 \lesssim S'_{K,\text{mosaic}}/\mu\text{Jy} \lesssim 3.6 \times 10^3$. We enlarged this range of validity slightly to $1.6 \lesssim S'_K/\mu\text{Jy} \lesssim 5.3 \times 10^3$ so that sector II now spans the range of stellar masses from 1 to $34 M_{\odot}$. A star of $M_* \sim 8 M_{\odot}$ has a reddened K -band flux density of $S'_K \sim 2 \times 10^2 \mu\text{Jy}$. It is of interest to note that in the region $5.3 \times 10^3 \lesssim S'_{K,\text{mosaic}}/\mu\text{Jy} \lesssim 10^5$, where the shifted BW KLF deviates from the power law approximation $\propto S'_K{}^{-0.8}$, the observations by DePoy et al. (1993), reduced as above and shown in Fig. 1, agree well with the observed mosaic KLF.

5. Physical plausibility of the mosaic KLF

The complete mosaic KLF, i.e. the combination of the model KLF sectors I + II with the observed KLF sectors III + IV, complies with conditions 1) and 3) stated in Sect. 4.1. Here we discuss condition 2), i.e. the physical plausibility of the model KLFs, by comparing observed and predicted stellar luminosities. The dust luminosity of the mosaic of $L_{\text{IR}} \sim 1.2 \times 10^8 L_{\odot}$ (Table C1) is clearly a lower limit to the stel-

lar luminosity. The K -band surface brightness integrated over the mosaic yields a comparable lower limit if we assume that all stars in the NB are old and evolved with an effective temperature of ~ 3000 K (see Eq. 12 below). The high Lyman continuum photon production rate derived from free-free radio emission (Table C1) indicates, however, that the stellar population of the NB contains a substantial fraction of young, massive and hot stars which can ionize the surrounding gas.

The predicted stellar luminosity depends on the number of massive MS stars which are mixed with evolved stars. For a separation of evolved and MS stars we can concentrate our efforts on sector II of the KLF which contains MS stars in the mass range $M_* \sim 1 - 34 M_{\odot}$. Sector I (which contain mainly MS stars with $M_* < 1 M_{\odot}$) as well as sectors III and IV (which contain mainly giants and supergiants) each contribute only $\sim 1/10$ -th of the estimated total stellar luminosity of $\sim 3.6 \times 10^8 L_{\odot}$ (see Table 2, bottom line). In the following we estimate the number of MS stars contained in sector II, labelling it as subgroup IIa and referring to the result as the Present Day Mass Function (PDMF).

5.1. Stellar luminosity of the mosaic

One can obtain a lower limit to the integrated luminosity of the ensemble of mosaic stars by assuming that all of these stars have effective temperatures as low as $T_{\text{eff}} \sim 3000$ K. Combination of Eqs. (5.4) and (5.5) of MDZ96 yields for the stellar luminosity (with $x = 6.55 \times 10^3 (\text{K}/T_{\text{eff}})$)

$$\left(\frac{L}{L_{\odot}}\right) = 7.14 \times 10^{-8} \left(\frac{T_{\text{eff}}}{\text{K}}\right)^3 \frac{e^x - 1}{x} \left(\frac{S_K}{\text{Jy}}\right) \quad (11)$$

and, specifically for the mosaic, we take $\tau_K \sim 3.2$, $S'_K \sim 752 \text{ Jy}$ and $S_K = S'_K e^{\tau_K} \sim 1.9 \times 10^4 \text{ Jy}$, obtaining

$$L_{*,\text{mosaic}} \gtrsim 1.3 \times 10^8 L_\odot \quad (12)$$

Likewise one obtains an upper limit for the luminosity by assuming that all stars in the KLF sector II are MS stars; the corresponding luminosity function dN_{II}/dL_* (Column 8 of Table 2) yields a cumulative luminosity of (see Column 9)

$$L_{*,\text{mosaic}} \lesssim 2.9 \times 10^{10} L_\odot \quad (13)$$

which we consider as a strict upper limit (actually this luminosity equals that of the whole Galactic Disk (see e.g. MDZ96, Table 5).

These lower and upper limits of the stellar luminosity in the central $\sim 30 \text{ pc}$ have to be compared to an estimated dust luminosity of $L_{\text{IR}} \sim 1.2 \times 10^8 L_\odot$ (Table C1, Column 2), which coincides with the lower limit given by Eq. (12). To conclude, however, that dust in the mosaic is mainly heated by cool stars would be wrong: since the dust absorption cross section in the NIR decreases $\propto \lambda^{-1.7}$ only a small fraction of the photons emitted by stars with $T_{\text{eff}} \sim 3000 \text{ K}$ will be intercepted by dust. The absorption by dust of radiation from hot stars is much more efficient. Furthermore, the presence of radio free-free emission (quantitatively represented by N'_{Lyc} , Table C1, Column 4; see also MDZ96) reveals convincingly the presence of hot and luminous stars in the mosaic outside the central parsec.

The upper limit of the integrated stellar luminosity of $L_{\text{IR}} \lesssim 3 \times 10^{10} L_\odot$ is ~ 250 times higher than the value of $\sim 1.2 \times 10^8 L_\odot$ consistent with both the observed dust luminosity (Table C1, Column 2) and the lower limit of the stellar luminosity (Eq. (12)). The reason for this high luminosity, contributed by medium and high mass MS stars, is the (physically implausible) assumption that all stars contained in sector II of the model KLF are actually still on the MS. In a more realistic approach one has to consider and account for the short MS lifetimes of the medium and high mass stars and therefore has to use the Present Day Mass Function (PDMF) rather than the IMF which describes the mass distribution of a newly born star generation. HST observations (Holtzmann et al., 1993) indicate for the central parsec a MS turnoff at stellar masses of $\sim 1 M_\odot$ which we adopt in the following discussion of the mosaic.

5.2. The present day mass function (PDMF)

In this section we search for a PDMF whose Lyc- and bolometric luminosity are consistent with the observations. In Appendix A, Eqs. (A.1) and (A.2) we give some integral properties of young O star clusters. Substitution of $N_{\text{Lyc}} \sim 3.6 \times 10^{51} \text{ s}^{-1}$ (Table C1, Column 6) for the actual Lyc photon production rate in Eq. (A.1) yields the mass $\langle M_* \rangle \sim 1.1 \times 10^4 M_\odot$ for the O star cluster responsible for the ionization of gas in the mosaic. This mass can be used to find the slope (for $M_* > 1 M_\odot$) of an appropriate PDMF. With $dN/dM_* = 2.73 \times 10^7 M_*^\alpha$ (see Table 2, Columns 9 and 10) the cumulative mass is

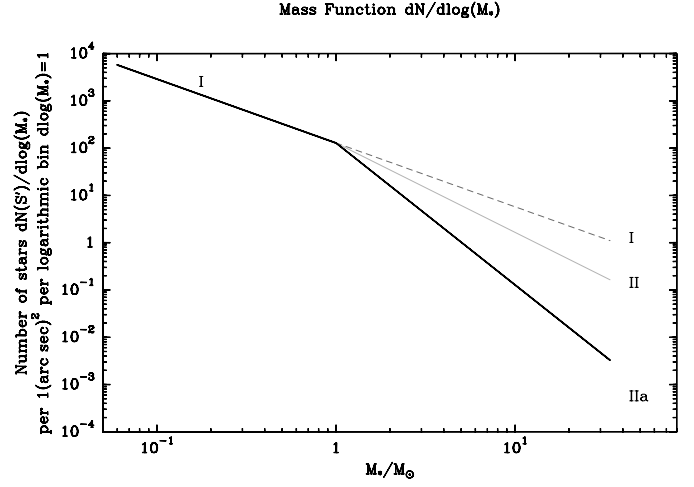


Fig. 2. Mass functions for MS stars in the mosaic discussed in this paper. The combination of the Salpeter IMF (sector I) with the PDMF (sector IIa) has been adopted (see Table 2, Column 10).

$$\frac{M_{\text{cum}}}{M_\odot} = 2.73 \times 10^7 \int_{M_* = 15 M_\odot}^{34 M_\odot} M_*^{\alpha+1} dM_* \quad (14)$$

The integration limits are determined by the fact that only O stars with masses $M_* \sim 15\text{--}34 M_\odot$ have high enough effective temperatures to contribute substantially to the ionization. Evaluation of the above Eq. (14) shows that for $\alpha \sim -4.5$ the cumulative mass is $\sim 1.36 \times 10^4 M_\odot$ sufficiently close to the above value $\langle M_* \rangle$. The corresponding cumulative bolometric luminosity of all O stars of $L_* \sim 2.8 \times 10^8 L_\odot$ is found in Table 2, Column 9, sector IIa together with the luminosity of all stars in the mosaic of $\Sigma_{\text{I}}^{\text{IV}} L_* \sim 3.6 \times 10^8 L_\odot$ which is $\sim 3L_{\text{IR}}$, the dust luminosity given in Table C1.

Fig. 2 shows the three different MFs which entered into the above discussion. $dN_{\text{I}}/d\log M_* \propto M_*^{-1.35}$ is the Salpeter IMF, which is the Present Day Mass Function (PDMF) of MS stars with $M_* \lesssim 1 M_\odot$. Similarly, $dN_{\text{II}}/d\log M_* \propto M_*^{-1.85}$ is the MF derived for the BW KLF adjusted for the stellar surface density of the central 30 pc. The mass and luminosity functions dN_{II}/dM_* and dN_{II}/dL_* , given in Columns 10 and 8 of Table 2, would hold if all stars in sector II of the KLF were MS stars. The much too high cumulative stellar luminosity of $\sim 2.9 \times 10^{10} L_\odot$ given in Column 9 shows that this assumption is unrealistic. To get agreement with observed luminosities we had to make the assumption that the stellar population in sector II consists of MS stars with a Present Day Mass Function (PDMF) $dN_{\text{IIa}}/dM_* \propto M_*^{-4.5}$ and evolved stars with the KLF II - IIa shown in Fig. 3 which account for the bulk of the observed K -band luminosity in sector II. This PDMF yields good agreement with the observed values L_* and N_{Lyc} . Its slope is also in agreement with the PDMF in the solar vicinity (see e.g. von Hoerner, 1968; Kroupa et al., 1993). We adopt for the following discussion $dN_{\text{I}}/dM_* + dN_{\text{IIa}}/dM_*$ as the Main Sequence PDMF of the central $\sim 30 \text{ pc}$ in the sectors I and II. This PDMF is shown as heavy solid line in Fig. 2.

Table 3. Numbers of main sequence stars ($1-34 M_{\odot}$), giants and supergiants contained in the mosaic

$M_{*,\min}$ M_{\odot} (1)	τ_{MS} yrs (2)	$M_{*,\max}$ M_{\odot} (3)	τ_{MS} yrs (4)	stars on MS [a] (5)	stars off MS [b] (6)	red giants [c] (7)	supergiants [d] (8)	stars not accounted for [e] (9)
1	$9.5 \cdot 10^9$	8	$1.3 \cdot 10^7$	$7.8 \cdot 10^6$	$1.1 \cdot 10^7$	$4.8 \cdot 10^5$		$6.6 \cdot 10^6$
8	$1.3 \cdot 10^7$	34	$4.2 \cdot 10^6$	$5.4 \cdot 10^3$	$1.0 \cdot 10^6$		$4.4 \cdot 10^4$	

τ_{MS} for $Z = 0.04$ from Schaerer et al. (1993). Accumulated numbers of stars have been computed from:

[a] dN_{IIa}/dM_*

[b] $dN_{\text{I}}/dM_* - dN_{\text{IIa}}/dM_*$; $dN_{\text{I}}/dM_* \propto M_*^{-2.35}$ is supposed to be the birthrate function (IMF).

[c] $dN_{\text{II}}/dS'_{\text{K}} - dN_{\text{IIa}}/dS'_{\text{K}}$ ($10^2 \lesssim S'_{\text{K}}/\mu\text{Jy} \lesssim 2 \times 10^3$)

[d] $dN_{\text{II}}/dS'_{\text{K}} - dN_{\text{IIa}}/dS'_{\text{K}}$ ($2 \times 10^3 \lesssim S'_{\text{K}}/\mu\text{Jy} \lesssim 5.3 \times 10^3$) + $N_{\text{cum III}} + N_{\text{cum IV}}$.

[e] $dN_{\text{II}}/dS'_{\text{K}} - dN_{\text{IIa}}/dS'_{\text{K}}$ ($1.6 \lesssim S'_{\text{K}}/\mu\text{Jy} \lesssim 100$).

The stellar mass contained in the mosaic had been assumed to be $\Sigma M_* \sim 1.2 \times 10^8 M_{\odot}$. The cumulative mass of MS stars (Table 2, Column 11), bottom) is slightly higher; however, a somewhat flatter IMF as suggested by Scalo (1986) will decrease the stellar mass contributed by sector I. The contribution of $N_* \sim 1.7 \times 10^4$ evolved stars (Column 5 sector III + IV) to the total mass should be negligible. The main contributors to the stellar mass (> 90%) are MS stars ($M_* \lesssim 1 M_{\odot}$) which account, however, for only $\sim 6\%$ of the integrated K band flux density of the mosaic. MS stars ($M_* > 1 M_{\odot}$) account for $\sim 7\%$ of the total mass, $\sim 6\%$ of the K band flux density but $\sim 80\%$ of the stellar luminosity of the mosaic.

5.3. The KLF of MS and evolved stars

Fig. 3 shows once more the complete mosaic KLF together with the KLF corresponding to the PDMF (Table 2, Column 3, sector IIa) which represents MS stars with $M_* > 1 M_{\odot}$. Also shown is the difference KLF $dN_{\text{II}}/d\log S'_{\text{K}} - dN_{\text{IIa}}/d\log S'_{\text{K}}$ which represents stars which have already moved off the MS. These stars clearly dominate the KLF in sector II. Only in the mass range around $M_* \sim 1-4 M_{\odot}$ do we find more MS stars than evolved ones.

In Table 3 we give the numbers of MS ($M_* > 1 M_{\odot}$) and evolved stars contained in the mosaic. Columns 1 through 4 give the range of stellar masses of MS stars together with the corresponding MS life times. The letters in brackets in the headings of Columns 5 through 8 refer to footnotes which indicate how the numbers of stars have been computed. Column 5 shows the number of stars still on the MS and Column 6 the number of stars which have moved off the MS since stars have formed in the NB. Remember that dN_{I}/dM_* is the Salpeter IMF which we adopt as an appropriate birth rate function in the NB and hence in sector II of the KLF.

MS stars with masses $\sim 1-8 M_{\odot}$ are supposed to evolve into red giants whose reddened flux densities range from $S'_{\text{K}} \sim 10^2$ to $2 \times 10^3 \mu\text{Jy}$ (Paper I, Fig. 9). Column 7 of Table 3 gives 4.8×10^5 as the number of stars which fall in this flux density range. This corresponds to $\sim 6\%$ of the MS stars in this mass range. Schaerer et al. (1993) have computed that the lifetimes of MS stars in the He-burning phases are about 10–20% of those

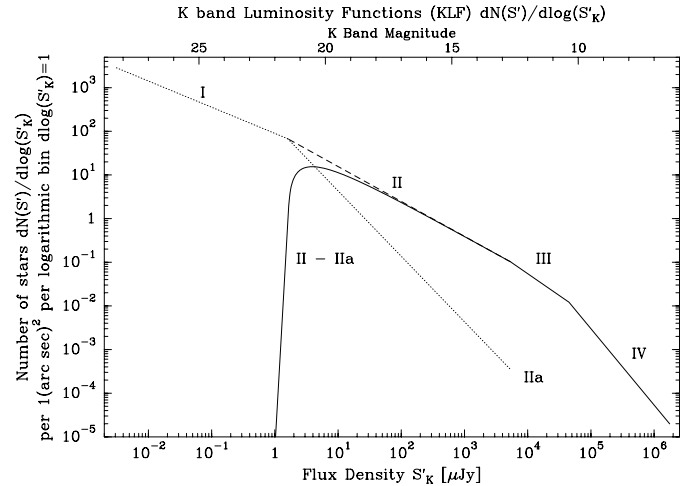


Fig. 3. The complete mosaic KLF (sectors I – IV from Fig. 1 together with sector IIa from Table 2, Column 3). Also shown is the difference KLF $dN_{\text{II}}/d\log S'_{\text{K}} - dN_{\text{IIa}}/d\log S'_{\text{K}}$ (see text) which represents stars which have moved off the MS. The light dotted curve indicates the KLF of MS stars, the heavy solid curve indicates the KLF of evolved stars.

in the H-burning phase. Massive MS stars in the range $M_* \sim 8 - 34 M_{\odot}$ are supposed to evolve through a short supergiant phase and to end as supernovae. Column 8 of Table 3 gives the number of 4.4×10^4 stars which could be evolved objects with progenitor masses $M_* \gtrsim 8 M_{\odot}$. There are, however, only $\sim 12\%$ of this number counted as MS stars. A much higher rate of formation of massive stars $\sim 10^7-10^8$ yrs ago (see below) would be a possible explanation of these numbers. There are also $\sim 6.6 \times 10^6$ additional stars with flux densities $1.6 \lesssim S'_{\text{K,BW}}/\mu\text{Jy} \lesssim 10^2$ which appear to be neither single MS stars nor to fit into the flux density range expected to be occupied by Red Giants. All these numbers should, however, be considered with caution since the KLF of sector II is not based on star counts in the mosaic but rather has been inferred from Baade's Window.

6. Star formation and stellar population in the central 30 pc

6.1. The overabundance of luminous stars at K

Several papers compare the KLF of the central parsecs with the KLF of Baade's Window (see Sect. 4.3 and references therein, Narayan et al. (1996), Blum et al. (1996)). Most authors agree that the KLF of the central parsecs has an overabundance of K -luminous stars, which are interpreted as remnants of high star formation activity some 10^7 to 10^8 yrs ago (Genzel et al. 1994; Tambllyn et al. 1996). We find for $S'_K \geq 5 \times 10^3$ Jy good agreement between the KLF derived here for the central 30 pc and the shifted BW KLF (see Fig. 1). In BW there are no stars observed with flux densities corresponding to $S'_{K, \text{mosaic}} \geq 10^5 \mu\text{Jy}$. This can be explained, however, as a purely statistical effect. The number of stars in the mosaic with $S'_K \geq 10^5 \mu\text{Jy}$ is ~ 358 . The KLF in BW is based on observations in a field of $2.58\hat{7}$ while the mosaic KLF covers a field of $128\hat{7}$. In Sect. 4.3, Eq. (10), we show that the stellar surface density in the NB is ~ 55.6 times higher than in BW. Hence, one expects in BW a surface density of stars with $S'_{K, \text{mosaic}} \geq 10^5 \mu\text{Jy}$ of only $3.6 \cdot 10^{-4} \times 358 \sim 0.13$ stars.

The difference KLFs shown in Paper I, Fig. 4b compare the NB KLF (Sgr A East minus M-0.13–0.08) with the GD KLF (M–0.13–0.08 minus Dark Cloud). Here the overabundance of K -luminous stars in the central 30 pc is clearly visible.

6.2. Bimodal star formation in the NB

In Appendix D we estimated star formation rates (SFRs) based on the Lyc photon production rate N_{Lyc} using procedures developed by Güsten & Mezger (1983, hereafter GM83). We obtain for a standard or continual Salpeter IMF an observed SFR of $\psi(t_0) \sim 0.9 M_\odot \text{ yr}^{-1}$ for the NB and $0.2 M_\odot \text{ yr}^{-1}$ for the mosaic. The observed SFR is even higher than the time-averaged SFR $\langle \psi \rangle = M_* / (1 - r) \tau_{\text{NB}} \sim 0.6 M_\odot \text{ yr}^{-1}$ of the NB with a total stellar mass $M_* \sim 4 \times 10^9 M_\odot$, an instantaneous return rate of $r \sim 0.3$ and an assumed age of the NB of $\tau_{\text{NB}} \sim 10^{10}$ yr. This result appears to suggest a constant SFR over the lifetime of the NB - a rather unlikely situation. GM83 had obtained similar contradictory results for the GD. These authors had introduced bimodal star formation to explain the abundance gradient observed in the ISM of the GD; as a by-product the concept of bimodal star formation also solved the apparent contradiction between time-averaged and present-day SFR. Bimodal star formation discriminates between spontaneous and induced star formation. In the GD spontaneous (i.e., normal) star formation occurs in dense clouds in the interarm region with a continual IMF including stars of all masses. Induced star formation occurs when ISM flows into spiral arms and gets compressed by density waves. In this case only stars above a critical mass $M_c \sim 1\text{--}5 M_\odot$ are formed. It is clear that in the case of bimodal star formation for a given Lyc photon production rate N_{Lyc} less ISM is converted into stars and an even lower fraction of ISM remains permanently locked-up in low-mass MS stars and

stellar remnants. Table D1 shows that for a specific bimodal model combining spontaneous and induced star formation, i.e. $M_c \sim 3 M_\odot$, $\psi_{\text{ind}} / (\psi_{\text{ind}} + \psi_{\text{spont}}) \sim 0.7$ for a given N_{Lyc} the SFR is reduced by a factor of 2.25 and the lock-up rate by a factor of 6. Alternatively we can state that in the case of bimodal star formation the luminosity per M_\odot converted into stars is between ~ 10 and 40 times higher (depending on M_c) than for star formation according to a continual IMF (see Mezger et al. 1974).

Our observations (Paper I Fig. 2b) show that for $R \leq 15''$ the contribution of K -band luminous (i.e. resolved) stars compared with that of low-luminosity (i.e. unresolved) stars is more than 80% but decreases to 50% at $R \sim 300''$. In the context of bimodal star formation this would mean that the ratio $\psi_{\text{ind}} / (\psi_{\text{ind}} + \psi_{\text{spont}})$ decreases with increasing distance from the GC. This suggestion is supported by Genzel et al. (1996) who find that in the central $24''$ early-type stars are concentrated in the central $12''$ while the brightest late-type stars, which are red supergiants and AGB stars, seem to avoid the central $4''$ and form a ring which peaks at $R \sim 7''$. This ring extends as far as $10''$ and appears to delineate the region of recent high-mass star formation. For the intermediate- and low-brightness stars Genzel et al. (1994) find a central depression. It is interesting to note that a bimodal star burst with $\langle \Psi \rangle \sim 1 M_\odot \text{ yr}^{-1}$ lasting for 5×10^6 yrs and producing mainly O stars would produce a luminosity of $\sim 2.5 \times 10^{10} L_\odot$, equaling the stellar luminosity of the GD. As already suggested by GM83, bimodal star formation could explain the extremely high central luminosities of starburst galaxies.

6.3. K -band luminosity as tracer of stellar mass

An evaluation of the KLF (Sect. 5.2) shows that low-mass stars ($M_* < 1 M_\odot$) contribute $> 90\%$ of the stellar mass but only $\sim 6\%$ of the integrated K -band flux density. If the populations of low-mass stars and red giants are not well mixed, the K -band surface brightness will not be proportional to the surface density of stellar mass. Fig. 6 of Paper I actually shows that the surface brightness of stars of medium and high luminosity stars at K is much more concentrated than that of the low-luminosity stars.

In Sect. 5.3 we assigned sectors IV, III, and part of sector II (viz. that for $S'_K \geq 100 \mu\text{Jy}$) to red giants and supergiants but were left with $\sim 6.6 \cdot 10^6$ stars with $1.6 \leq S'_K / \mu\text{Jy} \leq 100$ which could not be accounted for in terms of such stars (Column 9 of Table 3). These stars contribute ~ 122 Jy or $\sim 16\%$ to the integrated mosaic flux density of ~ 752 Jy. A similar discrepancy between observed K -band surface brightness and kinematic mass has already been noted by Maihara et al. (1978) and Hayakawa et al. (1977), who scaled the $\lambda 2.4 \mu\text{m}$ volume emissivity in the solar vicinity with Innanen's (1973) mass model (see e.g. Fig. III.7 in GM83). Serra et al. (1980) suggested that the excess NIR emission comes from M giants with progenitor stars of mass $M_* \sim 1.5\text{--}3 M_\odot$ together with an increased star formation rate some 10^8 to 10^9 yrs ago. As discussed above (see Sect. 5.3) such an explanation may also apply to the NB.

Table A1. Parameters of main sequence stars

Spectral Type	M_* M_\odot	T_{eff} K	L_* L_\odot	L_* L_\odot	N_{Lyc} s^{-1}	$S_{\text{K},*}$ μJy	$S'_{\text{K},*}$ μJy	
(1)	(2)	(3)	(4)	(5)	(6)	(7)	(8)	(9)
O4	34	$5.2 \cdot 10^4$	$1.05 \cdot 10^6$	$1.33 \cdot 10^6$	$1.02 \cdot 10^{50}$	$1.43 \cdot 10^5$	$5.8 \cdot 10^3$	$5.3 \cdot 10^3$
O6	24	$4.8 \cdot 10^4$	$3.94 \cdot 10^5$	$3.32 \cdot 10^5$	$2.38 \cdot 10^{49}$	$4.65 \cdot 10^4$	$1.9 \cdot 10^3$	$2.4 \cdot 10^3$
O8	17	$4.16 \cdot 10^4$	$1.03 \cdot 10^5$	$8.35 \cdot 10^4$	$4.90 \cdot 10^{48}$	$1.83 \cdot 10^4$	$7.5 \cdot 10^2$	$1.1 \cdot 10^3$
O9	15	$3.72 \cdot 10^4$	$6.38 \cdot 10^4$	$5.06 \cdot 10^4$	$2.12 \cdot 10^{48}$	$1.59 \cdot 10^4$	$6.5 \cdot 10^2$	$8.1 \cdot 10^2$
B0	13	$3.22 \cdot 10^4$	$3.45 \cdot 10^4$	$2.86 \cdot 10^4$	$4.17 \cdot 10^{47}$	$1.24 \cdot 10^4$	$5.1 \cdot 10^2$	$5.8 \cdot 10^2$
B5	5.0	$1.64 \cdot 10^4$	$7.14 \cdot 10^2$	$6.25 \cdot 10^2$	$1.48 \cdot 10^{43}$	$1.82 \cdot 10^3$	$7.4 \cdot 10^1$	$6.5 \cdot 10^1$
A0	2.8	$1.08 \cdot 10^4$	$7.19 \cdot 10^1$	$6.15 \cdot 10^1$		$5.77 \cdot 10^2$	$2.4 \cdot 10^1$	$1.7 \cdot 10^1$
A5	2.0	$8.62 \cdot 10^3$	$1.73 \cdot 10^1$	$1.60 \cdot 10^1$		$2.49 \cdot 10^2$	$1.0 \cdot 10^1$	7.9
G0	1.1	$5.92 \cdot 10^3$	1.45	1.46		$5.30 \cdot 10^1$	2.2	2.0
K5	0.6	$3.97 \cdot 10^3$	$2.01 \cdot 10^{-1}$	$2.39 \cdot 10^{-1}$		$1.75 \cdot 10^1$	$7.1 \cdot 10^{-1}$	$4.9 \cdot 10^{-1}$
M8	0.06	$2.6 \cdot 10^3$	$1.0 \cdot 10^{-3}$	$3.79 \cdot 10^{-4}$		$7.68 \cdot 10^{-2}$	$3.1 \cdot 10^{-3}$	$2.5 \cdot 10^{-3}$

Acknowledgements. The data reductions and analyses were carried out on workstations provided by the *Alfried Krupp von Bohlen und Halbach Stiftung* through a joint grant to the Max-Planck-Institut für Radioastronomie and the Institut für Theoretische Astrophysik, University of Heidelberg. This support is gratefully acknowledged. We benefitted much from discussions with P.L. Biermann, W.J. Duschl and R. Kudritzki; our special thanks go to I.S. Glass whose suggestions substantially improved this paper.

Appendix A: mass-luminosity relations

Parameters of a number of stars of different spectral type are compiled in Table A1. For stars O4 through K5 we use the stellar parameters given by Mezger et al. (1974); for M8 we use the stellar parameters given by Lang (1992).

The K band luminosities $S_{\text{K},*}$ in Column 7 of Table A1 have been computed with Eqs. 5.4 from MDZ96 using a distance $R_0 \sim 8.5$ kpc to the Galactic Center. The reddened flux density $S'_K = e^{-\tau_K} S_K$ in Column 8 of Table A1 has been computed for $\tau_K \sim 3.2$, which corresponds to a visual extinction $A_V \sim 31$ mag. In Column 9 we give the approximate flux densities computed with Eq. (4).

The stellar luminosities of Mezger et al. (1974) in Column 4 should be compared with the approximation given in Column 5 computed with Eq. (6).

In the following we also make use of integral properties of young OB star clusters. Mezger et al. (1974) give for stars earlier than B0

$$\frac{\langle N_{\text{Lyc}} \rangle}{\langle M_* \rangle} = 3.16 \times 10^{47} \quad \text{photons per s and } M_\odot \quad (\text{A1})$$

and

$$\frac{\langle L_* \rangle}{\langle M_* \rangle} = 5.38 \times 10^3 L_\odot \text{ per } M_\odot \quad (\text{A2})$$

Appendix B: how to convert mass into luminosity functions and vice versa

In Sect. 3 we gave each of the MF, LF and KLF in a general algebraic form. The exponents are related by

Table B1. Combinations of exponents

Eq. (3) α	Eq. (4) β_1	Eq. (6) β_2	Eq. (2) γ_1	Eq. (2) $\gamma_1 + 1$	Eq. (5) γ_2
-2.35	2.3		-1.6	-0.6	
		2.8 4.0			-1.5 -1.35
-2.85	2.3		-1.8	-0.8	
		2.8 4.0			-1.65 -1.45
-4.50	2.3		-2.50	-1.50	
		2.8 4.0			-2.25 -1.85

$$\gamma_1 = \frac{\alpha - \beta_1 + 1}{\beta_1} \quad (\text{B1})$$

$$\gamma_2 = \frac{\alpha - \beta_2 + 1}{\beta_2} \quad (\text{B2})$$

The constants are related by

$$C_1 = \frac{A}{\beta_1 B_1^{\gamma+1}} \quad (\text{B3})$$

$$C_2 = \frac{A}{\beta_2 B_2^{\gamma+1}} \quad (\text{B4})$$

with $\beta_1 = 2.3$, $B_1 = 1.6$ and $\beta_2 = 2.8$ or 4.0 (see Eq. (6)) and $B_2 = 1$. Some combinations of α , β and γ used to compute MFs, LFs and KLFs in Table 2 are given in Table B1. Remember that the exponent of the logarithmic KLF is $\gamma + 1$.

Appendix C: dust luminosity and Lyc-photon production rate in the mosaic

To check the stellar luminosities (L_*) computed in Sect. 5.1 it is important to estimate the dust luminosity L_{IR} and the Lyc-photon production rate N_{Lyc} integrated over the mosaic. There is

Table C1. IR-luminosity and Lyc-photon production rate related to central pc, the mosaic, and the nuclear bulge

R arcsec (1)	L_{IR} L_{\odot} (2)	Ref. (3)	N'_{Lyc} s^{-1} (4)	Ref. (5)	N_{Lyc} s^{-1} (6)	Ref. (7)
$1.5 \cdot 10^1$	$3.7 \cdot 10^6$	[a]	$6.3 \cdot 10^{49}$	[b]	$1.9 \cdot 10^{50}$	[e]
$3.83 \cdot 10^2$	$1.2 \cdot 10^8$	[c]	$1.2 \cdot 10^{51}$	[d]	$3.6 \cdot 10^{51}$	[e]
$3.04 \cdot 10^3$	$1.3 \cdot 10^9$	[b]	$6.4 \cdot 10^{51}$	[b]	$1.9 \cdot 10^{52}$	[e]

References:

[a] Paper I, Table 1b (Note that in Paper I Table 1c the IR luminosity (corr.) of $(7.5 \pm 3.5) \cdot 10^7 L_{\odot}$ relates to the stellar luminosity.

[b] see MDZ96, Table 6 and references therein.

[c] Interpolated with $L_{\text{IR}} \propto R^{1.1}$.

[d] Interpolated with $N'_{\text{Lyc}} \propto R^{0.9}$.

[e] Correction for Lyc-Photons directly absorbed by dust $N_{\text{Lyc}} \sim 3N'_{\text{Lyc}}$ (see Mezger & Pauls, 1978).

an unpublished dust luminosity $L_{\text{IR}} \sim 4.4 \times 10^7 L_{\odot}$ derived by Launhardt from COBE-DIRBE and IRAS observations but there are no observations of N'_{Lyc} (i.e. the number of Lyc-photons directly absorbed by the interstellar gas which contribute to the radio free-free emission) and L_{IR} available which would relate directly to the mosaic; the corresponding values in Table C1 have therefore been interpolated between measurements related to the central $R \lesssim 15''$ and to the NB ($R \lesssim 3 \times 10^{3''}$; see MDZ96 and Paper I). Column 1 gives the radii adopted for the central 30 pc, mosaic and Nuclear Bulge (in l).

Appendix D: star formation and lock-up rates

The star formation rate (SFR) $\psi(t)$ is the rate at which ISM is transformed into stars. Stars with masses $M_* > 1 M_{\odot}$ have MS lifetimes shorter than the age of the GD (assumed to be $\tau_{\text{GD}} \sim 10^{10}$ yr). They evolve to giants and supergiants, loose part of their outer shell to the ISM and end as white dwarfs, neutron stars, or black holes. With $r \sim 0.3$, the fraction of matter instantaneously returned to the ISM by a new generation of stars, the lock-up rate $(1-r)\psi(t)$ is the fraction of matter transformed into stars which is permanently locked up in low-mass stars ($M^* < 1 M_{\odot}$) and in the remnants of massive stars. The average star formation rate in the NB is then

$$\langle \psi(t) \rangle = \frac{M_*}{(1-r)\tau_{\text{NB}}} \sim 0.6 M_{\odot} \text{ yr}^{-1} \quad (\text{D1})$$

with $M_* \sim 4 \cdot 10^9 M_{\odot}$ the total stellar mass and $\tau_{\text{NB}} \sim \tau_{\text{GD}} \sim 10^{10}$ yrs the age of the NB. For a closed system and a SFR proportional to the mass of ISM available, $\psi \propto M_{\text{ISM}}$, Güsten & Mezger (1983; in the following referred to as GM83) give a relation between present-day and time-averaged SFR:

$$\frac{\psi(t_0)}{\langle \psi \rangle} = \frac{\mu \ln \mu^{-1}}{(1-\mu)} = 9 \cdot 10^{-2} \quad (\text{D2})$$

which - with $M_{\text{ISM}} \sim 10^8 M_{\odot}$ and $\mu = M_{\text{ISM}}/(M_* + M_{\text{ISM}}) \sim 0.024$ - predicts a present-day SFR $\psi(t_0)_{\text{pred}} \sim 6 \cdot 10^{-2} M_{\odot} \text{ yr}^{-1}$. On the other hand, if one estimates the SFR

Table D1. Star formation and lock-up rates in the GD, GB, and in the central 30 pc

	Galactic Disk $M_{\odot} \text{ yr}^{-1}$		Nuclear Bulge $M_{\odot} \text{ yr}^{-1}$		Mosaic $M_{\odot} \text{ yr}^{-1}$	
	ψ (1)	$\psi(1-r)$ (2)	ψ (3)	$\psi(1-r)$ (4)	ψ (5)	$\psi(1-r)$ (6)
contin. IMF	9.4	6.5	0.9	0.6	0.2	0.1
bimod. IMF	4.3	1.1	0.4	0.1	0.08	0.02

Remarks:

[a] GM83. *Continual IMF* refers to Salpeter IMF, *bimodal IMF* has the following parameters: $M_c \sim 3 M_{\odot}$; $\psi_{\text{(ind)}}/\psi_{\text{(spont+ind)}} \sim 0.7$.

[b] Scaled with $N(\text{NB})/N(\text{GD})$ and $N(\text{mos})/N(\text{GD})$ with $N(\text{NB})$ and $N(\text{mos})$ given in Table C1 and $N(\text{GD}) \sim 2.0 \cdot 10^{53}$ given above.

from the Lyc photon production rate, one obtains a present-day SFR (see GM83 and Table D1) of $\psi(t_0)_{\text{obs}} \sim 0.9 M_{\odot} \text{ yr}^{-1}$, which is ~ 15 times higher than the predicted SFR and close to the time-averaged SFR given above (Eq. D1).

As discussed above (see Sect. 6.2) GM83 found that bimodal star formation could solve this problem. SFR and lock-up rates for the GD as derived by GM83 are given in Table D1, Columns 1 and 2 for $M_c \sim 3 M_{\odot}$. The corresponding rates for the NB and the Mosaic, scaled according to their Lyc-Photon production rate N_{Lyc} , are given in Columns 3 through 6.

References

- Blum R.D., Sellgren K., DePoy D.L., 1996, ApJ 470, 864
 Davidge T., 1991, ApJ 380, 116
 Davidge T., Simons D.A., Rigaut F., Doyon R., Crampton D., 1997, AJ 114, 2586
 DePoy D.L., Terndrup D. M., Frogel J.A., et al., 1993, AJ 105, 2121
 Genzel R., Hollenbach D., Townes C.H., 1994, Rep. Prog. Physics 57, 417
 Genzel R., Thatte N., Krabbe A., Kroker H., Tacconi-Garman L.E., 1996, ApJ 472, 153
 Genzel R., Eckart A., Ott T., Eisenhauer F., et al., 1997, MNRAS 291, 219
 Güsten R., Mezger P.G., 1983, Vistas in Astronomy 26, 159 (GM83)
 Hayakawa S., Ho K., Matsumoto T., Uyama K., 1977, A&A 58, 325
 von Hoerner S., 1968, In: Terzian Y. (ed.) Proc. Interstellar Hydrogen. 101
 Holtzmann J.A., Light R.M., Baum W.A., et al., 1993, AJ 106, 1826
 Innanen K.A., 1973, Ap&SS 22, 293
 Kroupa P., Tout C.A., Gilmore G., 1993, MNRAS 262, 545
 Lang K.R., 1992, Astrophysical Data: Planets and Stars. 132ff.
 Maihara T., Oda N., Sugiyama T., Okudu H., 1978, PASJ 30, 1
 Mezger P.G., Smith L.F., Churchwell E., 1974, A&A 32, 269
 Mezger P.G., Pauls T., 1978, IAU-Symp. 84, 357
 Mezger P.G., Duschl W.J., Zylka R., 1996, A&AR 7, 289 (MDZ96)
 Narayan V.K., Gould A., DePoy D.L., 1996, ApJ 472, 183
 Philipp S., Zylka R., Mezger P.G. et al., 1999, A&A in press (Paper I)
 Scalo J.M., 1986, Fund. Cos. Phys. 11, 1
 Schaerer D., Charbonnel G., Maynet G., et al., 1993, A&AS 102, 339
 Serabyn E., Morris M., 1996, Nat 382, 602
 Serra G., Puget J.L., Ryter C.E., 1980, A&A 84, 220
 Tamblyn P., Rieke G.H., Hanson M.M. et al., 1996, ApJ 456, 206
 Tiede G.P., Frogel J.A., Terndrup, D.M., 1995, AJ 110, 2788